International Journal of Electrical, Electronic and Communication Sciences
ISSN: 2517-9438
Vol:6, No:9, 2012

Silicon-based Low-Power Reconfigurable Optical Add-Drop Multiplexer (ROADM)

Junfeng Song, Xianshu Luo, Qing Fang, Lianxi Jia, Xiaoguang Tu,Tsung-Yang Liow, Mingbin Yu, Guo-Qiang Lo

***Abstract*—**We demonstrate a 1×4 coarse wavelength division-multiplexing (CWDM) planar concave grating multiplexer/demultiplexer and its application in re-configurable optical add/drop multiplexer (ROADM) system in silicon-on-insulator substrate. The wavelengths of the demonstrated concave grating multiplexer align well with the ITU-T standard. We demonstrate a prototype of ROADM comprising two such concave gratings and four wide-band thermo-optical MZI switches. Undercut technology which removes the underneath silicon substrate is adopted in optical switches in order to minimize the operation power. For all the thermal heaters, the operation voltage is smaller than 1.5 V, and the switch power is ~2.4 mW. High throughput pseudorandom binary sequence (PRBS) data transmission with up to 100 Gb/s is demonstrated, showing the high-performance ROADM functionality.

***Keywords*—**ROADM, Optical switch, low power consumption, Integrated devices.

I. Introduction

OPTICAL communications system has been widely used as the information transmission system, owing to the advantages of large data bandwidth, high security and low power consumption. In order to further enhance the data transmission capacity, wavelength-division multiplexing (WDM) technology has been introduced. In general, WDM can be divided into two wavelength patterns, namely, the coarse WDM (CWDM) with up to eight channels and wide channel spacing, and the dense WDM (DWDM) with large number of optical channels and narrow channel spacing. In comparison, the CWDM system becomes first choice for metropolitan area networks, benefiting from its low cost in equipments, operation and maintenance [1, 2]. In fact, CWDM is potentially applicable for on-chip optical interconnect in date center. This is because, on one hand, CWDM has same functions as general WDM system, can extend band width for increased date throughput. On the other hand, it adopts cooling-free laser source with large wavelength tolerance, thus significantly reducing the cost. Refer to development of optical communication systems, on-chip optical interconnect will need similar functional components, such as reconfigurable optical add/drop multiplexing (ROADM). In general, array waveguide grating (AWG) or concave grating can be employed as multiplexer/demultiplexer (MUX/DEMUX) components for ROADM.

Junfeng Song, Xianshu Luo, Qing Fang, Lianxi Jia, Xiaoguang Tu, Tsung-Yang Liow, Mingbin Yu, Guo-Qiang Lo are with the Institute of Microelectronics, A*STAR (Agency for Science, Technology and Research), Singapore, 117685, e-mail: songjf@ ime.a-star.edu.sg).

Junfeng Song is also with State Key Laboratory on Integrated opto-electronics, College of Electronic Science and Engineering, Jilin University, Changchun, People's Republic of China, 130012.

As the concave grating has the advantage of compact footprint and thus offers high integration density, it is believed to be more suitable for low power consumption and very large scale on-chip integration.

Meanwhile, silicon-on-insulator (SOI) waveguide allows high optical mode confinement due to large index contrast between silicon and silicon dioxide, thereby allowing the realization of compact optical devices and circuits. Together with the technology process development, SOI-based optical devices are deemed to play important roles in telecommunications and on-chip optical networking applications. Moreover, leveraging on mature Si-CMOS technology, ultra-compact and complex electronically controlled photonic devices can be expected. Therefore, SOI-based CWDM systems appear to be attractive [3-6].

In this paper, we demonstrate a low-power ROADM in SOI comprising two concave gratings as the MUX/DEMUX and four Mech-Zehnder interferometers (MZIs) based wide-band thermo-optical switches. We demonstrate a 1×4 concave grating following such design with the channel wavelength aligning to the ITU-T standard. By using such concave gratings, we demonstrate a thermo-optical tunable ROADM system. In order to minimize the switching power, undercut structure is adopted by removing the underneath silicon substrate. For all the thermal heaters, the operation voltage is smaller than 1.5 V, and the switch power is ~2.4 mW. High throughput pseudorandom binary sequence (PRBS) data transmission with up to 100 Gb/s is demonstrated, showing the high-performance ROADM functionality.

II. Design, Fabrication and Characterizations

A. Design

In a SOI platform, it is important to consider the effect of silicon waveguide thickness variation as the refractive index contrast is large. The waveguide thickness affects the effective refractive index, n_{eff}, which finally affects the optical performances of the concave grating. Here we use an effective index method to investigate the effect of the waveguide thickness to the effective refractive index by assuming a SiO_2/Si/SiO_2 sandwiched waveguide structure with consideration of the dispersion of Si and SiO_2.

Figure 1(a) shows the calculated effective refractive index as function of waveguide thickness for both fundamental and first-order modes. The red circle denotes the waveguide thickness of 220 nm, which corresponding to the SOI wafer we adopted. For silicon waveguide thickness thinner than 245 nm, the waveguide remain single mode. We also see that the effective refractive index is sensitive to the waveguide thickness, especially at ~ 220 nm region.

Figure 1(b) shows the effective refractive index change to the waveguide thickness, which would result in the wavelength shift, as described,

$$\frac{\partial n}{\partial d}\frac{\lambda}{n_g} = \frac{\Delta\lambda}{\Delta d} \quad (1)$$

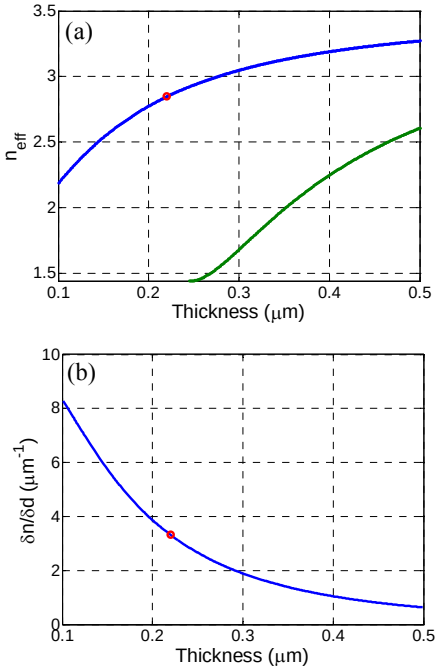

Fig. 1 (a) Waveguide effective index as the functions of waveguide thickness for both fundamental and first-order modes at 1.55 μm. (b) Effective changing rate as the function of waveguide thickness. Red circle illustrate the waveguide thickness of 0.22 μm

Based on the calculation of Fig. 1(a) and (b), we can attain the effective index of 220 nm thick silicon waveguide of n_{eff}= 2.85, $n_g \approx 3.7$, and $\delta n/\delta d \approx 3.3$. Thus, we have $\Delta\lambda/\Delta d \approx 1.38$. This suggests that for only 1 nm thickness change, the wavelength shift is ~ 1.38 nm.

From the calculation, we can determine the structure parameters of a concave grating by using recursive modeling method [8, 9]. For a four-channel concave grating with channel wavelengths of 1531 nm, 1551, nm, 1571, nm, and 1591 nm, the radius of the grating circle is 188 μm. The incident light point is with 41° angle to original point, which is the cross point of the grating circle and *x* axis. The order number *m* is 10. In order to reduce the reflection loss at the grating circle, we adopt the planar Brag grating structure, which is designed by using Si/SiO_2 (410 nm/286 nm) structures. The reflectivity is larger than 99% if the period number of Bragg grating is larger than 4. Here we adopt 7 periods to ensure smaller reflection loss.

B. Device Fabrication

Following the CMOS compatible optical thermal devices fabrication process [10], we start the fabrication on a commercially available 200 mm SOI wafer with 220 nm-thick top silicon and 2 μm-thick buried oxides.

The wafer is first covered by depositing 50 nm undoped silicate glass oxide (USG) as the hard mask, followed by 248 nm deep UV photolithography to pattern the device and the hard mask etch by plasma reactive ion etching (RIE) process. Two step RIE etching is performed for both channel and slab waveguide. The remained slab thickness is ~ 70 nm. This technology makes ridge waveguide in order to reduce the light couple between sandwiched slab waveguide and channel waveguide. Spot size converters (SSCs) are fabricated at the input and output coupling facets in order to reduce the coupling losses between fiber to waveguide and vice versa. These SSCs are nano-tapers with 200 nm-wide tips and 200 μm in length. Then ~1.5 μm high-density plasma (HDP) oxide is deposited, followed by 150 nm Titanium nitride (TiN) deposition for the thermal heater. A 30 nm-thick silicon nitride is deposited for TiN etching protection. After the formation of contact holes, ~750 nm thick aluminum is deposited, followed by metal pad etching. Finally, two kinds of deep trenches are formed, one of which serves as thermal isolation by etching holes around thermally tunable waveguides. This is used for reducing the switching power [11]. Another one is a 100-μm wide trench at both sides of the chips for fiber end-coupling [12]. For the same chip, we also include standing alone concave grating and thermo-optical tunable MZI switch for reference which are designed identically with those in the ROADM.

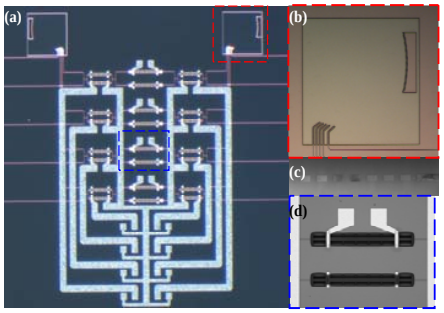

Fig. 2 Optical micrographs of the fabricated (a) 1 × 4 ROADM, and (b) the concave grating. (c) TEM of the cross sectional view of the DBR mirror. (d) The thermo-optically tunable MZI switch. The dark regions along the MZI arms are the isolation deep trenches

Figure 2(a) shows the optical micrograph of the fabricated 1 × 4 ROADM, comprising two 1 × 4 concave gratings as MUX/DEMUX and four wideband thermally tunable MZI switches. For each of the MZI switches, we adopt 3rd-order cascaded MZIs for the 2×2 switches, in which the first and the third MZIs being designed to achieve the 3-dB couplers with wide bandwidth and thermal tunability, while the second MZI functions for optical switching by thermo-optical effect. As the ROADM usually works in a very wide wavelength range and the conventional 3 dB directional coupler only works within very short wavelength range, we adopt two thermally tunable MZI structure serves as the input/output 3-dB couplers. In our case, each switch working for one of wavelength (band width <10 nm), the thermal tuning of 3-dB will make every optical switch working on the best status. In this way, we can easily adjust it to achieve idea 3-dB coupling.

Figure 2(b) shows the zoom-in view of the concave grating. The seven-period DBR mirror is adopted at the grating circle, whose cross section is shown in Fig. 2(c). Figure 2(d) shows the thermo-optically tunable MZI switch with the dark region being the deep trenches. The MZIs are with the waveguide width of 400 nm and the length of directional coupler of 11 μm. The gaps between the waveguides for the directional coupler are 300 nm.

C. Characterizations

We first characterize the standing alone components, namely the concave grating and the wideband MZI thermo-optical switches. Figure 3 shows the measured TE-polarized transmission spectra of the concave grating for all four channels. The channel center wavelengths locate at 1531, 1551, 1571, and 1591 nm, which align with the ITU-T standard very well.

The transmission loss is smaller than ~4 dB (normalized by straight reference waveguide) with the input/output coupling loss of SSC is ~3 dB. The loss non-uniformity among four channels is < 2 dB. For 220 × 400 nm Si waveguide covered by SiO2, the transmission loss is 2.5~2.8 dB/cm.

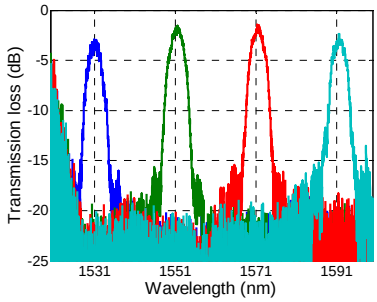

Fig. 3 Measured transmission spectra of the standing alone 1 × 4 concave grating. The transmission band wavelengths locate at 1531, 1551, 1571, and 1591 nm

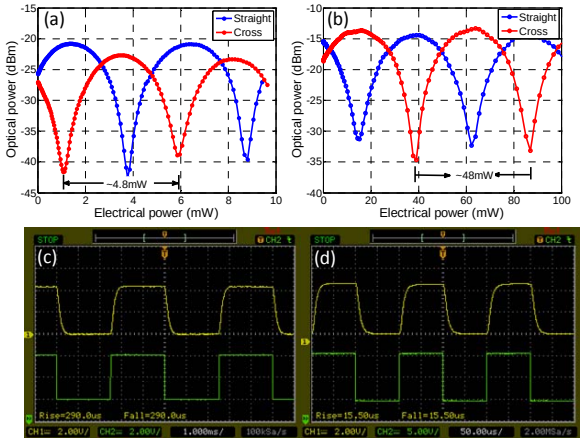

Fig. 4 (a), (b) Optical responses upon different electrical powers for the MZI switch with and without thermal isolation. (c), (d) Time responses for the MZI switch with and without thermal isolation. Yellow lines: Optical response. Green lines: Electrical input

We investigate the switch performances by measuring the optical response upon DC voltage supply at fixed carrier wavelength of 1550 nm.

Figure 4(a) shows the measured optical response as the function of the applied electrical power for both bar and cross transmissions. The electrical power is calculated based on the Current-Voltage curves. The heater resisters for the input and output 3-dB couplers are ~171 Ω, while for the center MZI switch is ~230 Ω.

The required electrical power for π phase shift is only ~4.8 mW, corresponding to a switch power of only ~2.4 mW. Such low power consumption is due to the air trench underneath which confine the heat in the waveguide region with minimum dissipation. The 3rd order MZI optical switch without deep trench structure will induces ~2 dB additional loss. We attribute the non-uniform losses for bar and cross transmissions to the non-optimized 3-dB couplers. The on-off ratio is ~20 dB.

For comparison, we also measured the identically designed MZI switch without thermal isolation deep trench underneath. Both switches are fabricated in the same wafer but different wafer sides. Figure 5(b) shows the measured optical responses. The required electrical power for π phase shift is ~48 mW, which is one order higher than that of with deep trench.

Optical dynamic responses are investigated for both types of switches by modulating the thermo-optical switches with low-speed electrical signals. Figure 4(c) and (d) show the measurement results. We mention that the modulating speeds are 400 Hz and 10 KHz to the switches with and without deep trench in order to clearly display the rise/fall times. The measured rise/fall times for the switch with deep trench is ~290/290 μs, while for the switch without deep trench is ~15.5/15.5 μs. For the switch with deep trench, although the electrical power reduces significantly, the corresponding switching time is increased due to the reduced supplied electrical power. However, for most of the applications, the switch power requirement is much critical than the switching time. Thus, in the following discussion, we will only focus on the low power consumption switch with deep trench.

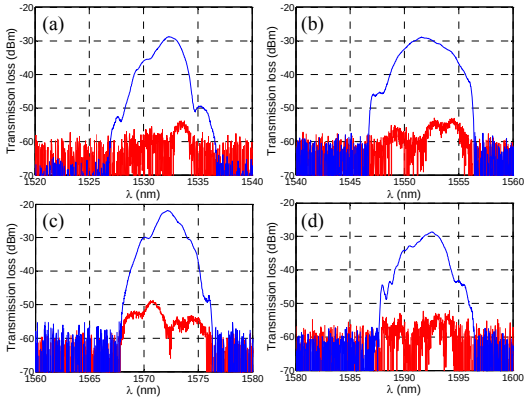

Fig. 5 The measured transmission spectra for all four channels at on/off status. (a) channel 1 at 1531 nm. (b) channel 2 at 1551 nm. (c) channel 3 at 1571 nm. (d) channel 1 at 1591 nm.

We then investigate the performances of the demonstrated ROADM, which comprising the demonstrated concave grating and MZI switches. Figure 5(a)-(d) show the measured transmission spectra for all four channels at on/off status.

The 3-dB bandwidths are >1.8 nm and the on-off ratios for all four channels are ~30 dB, suggesting perfect switching performance. However, the optical performances vary among the channels, especially the transmission band shapes. We attribute such deviations to the aggregated fabrication imperfections from the concave grating, unbalanced MZI, and the 3-dB couplers.

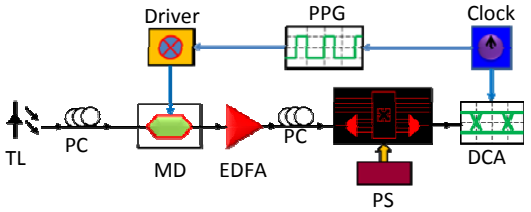

Fig. 6 Experimental Ssetup for signal transmission characterizationfor ROADM signal transmission characterization. TL: tunable laser; PC: polarization controller; MD: LiNbO3 optical modulator; PS: power supply; DCA: digital communication analyzeroscilloscope; PPG: programmable pattern generator

We also measure the signal transmission by passing a 25 Gbit/s PRBS optical signal (bit length 2^{31}-1) through the ROADM. The carrier wavelengths are chosen to align with the center of the optical channels. Figure 6 shows the measurement setup. A continuous-wave laser output at selected carrier wavelength is modulated at a signal with data rate of 25 Gbit/s that are generated by a programmable pattern generator (PPG) and a 4-channel multiplexer (MUX). The light is then amplified by an Erbium Doped Fiber Amplifier (EDFA) to boost the optical power before sending into the ROADM through a polarization-maintenance single-mode lensed-fiber. The polarization is controlled to be TE polarization by an optical polarization controller. The output signal from the device is collected by another single-mode lensed fiber and finally displayed in a large-bandwidth (up to 65 GHz) digital communication analyzer (DCA).

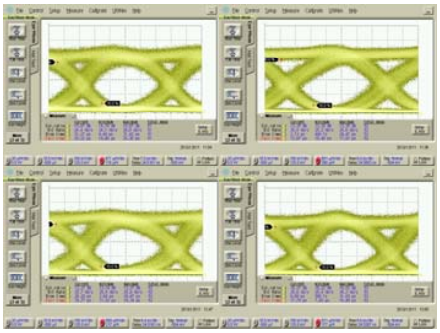

Fig. 7 Eye diagrams of the transmitted 25 Gbit/s PRBS signals (2^{31}-1) for all four channels from the ROADM. The extinction ratios are all larger than 13 Db

Figure 7 show the measured eye diagrams of the transmitted 25 Gbit/s PRBS signals for all four channels from the ROADM. The open eye diagrams suggest the high-quality data switching and transmission. For all the measured eye diagrams, the extinction ratios are exceeding 13 dB while the peak-to-peak jitters are ~ 10 ps. Such demonstrations suggest high-throughput of up to 100 Gb/s data transmission capability.

However, the signal-to-noise ratios are relatively low due to the relative high insertion loss accumulated from the whole optical link, which degrades the transmitted signal quality.

III. Conclusion

We demonstrated a silicon-based 1×4 low-power reconfigurable optical add-drop multiplexer (ROADM) using concave grating as the MUX/DEMUX. The optical switch is realized by using thermo-optically tunable third-order cascaded Mech-Zenhder interferometer in order to obtain wide wavelength bandwidth with less than 1.5 V DC tuning voltage and only ~ 2.4 mW switching power. High-throughput transmission is demonstrated by transmitting 25 Gb/s PRBS signals through the ROADM.

Acknowledgment

This work was supported by the Science and Engineering Research Council of A*STAR (Agency for Science, Technology and Research), Singapore under SERC grant number: 1021740174. And program for New Century Excellent Talents in University (NCETU), Nature Science Funding of China, NSFC (61177090).

References

[1] H. Zimmermann, Integrated Silicon Optoelectronics, Springer, New York, 2000.
[2] Banerjee, Y. Park, F. Clarke, H. Song, S. Yang, G. Kramer, K. Kim and B. Mukherjee, "Wavelength-division-multiplexed passive optical network (WDM-PON) technologies for broadband access: a review," J. Opt. Netw. 4, pp.737-758 (2005).
[3] J. Brouckaert, W. Bogaerts, P. Dumon, D. Van Thourhout, and R. Baets, "Planar concave grating demultiplexer fabricated on a nanophotonic silicon-on-insulator platform," J. Lightwave Technol. 25, pp.1269-1275 (2007).
[4] J. Brouckaert, G. Roelkens, S. K. Selvaraja, W. Bogaerts, P. Dumon, S. Verstuyft, D. Van Thourhout and R. Baets, "Silicon-on-insulator CWDM power monitor/receiver with integrated thin-film InGaAs photodetectors," IEEE Photon. Technol. Lett. 21, pp.1423-1435 (2009) .
[5] Dipak Chowdhury, "Design of low-loss and polarization-insensitive reflection grating-based planar demultiplexers," IEEE J. Sel. Top. Quantum Electron. 6, pp.233-235 (2000).
[6] R. Doerr, M. Cappuzzo, L. Gomez, E. Chen, A. Wong-Foy, C. Ho, J. Lam, and K. McGreer, "Planar lightwave circuit eight-channel cwd multiplexer with <3.9-db insertion loss," J. Lightwave Technol. 23 pp.62-65 (2005).
[7] K. A. McGeer. "Theory of concave gratings on a recursive definition of facet positions," Appl. Opt. 35, pp.5904-5910 (1996).
[8] J. Song, Q. Fang, T. Liow, H. Cai, M. Yu, G. Lo, and D. Kwong, "CWDM Planar Concave Grating Multiplexer/Demultiplexer and Application in ROADM," in Optical Fiber Communication Conference, OSA Technical Digest (CD) (Optical Society of America, 2011), paper JThA020.
[9] J. Song, X. Luo, Q. Fang, T. -Y. Liow , H. Cai, M. -B. Yu, and G. -Q. Lo, "Low Aberration Concave Grating for Re-configurable Optical Add/Drop Multiplexer Applications," in proceedings of IEEE MWP/APMP 2011, Singapore, 2011.
[10] J. Song, Q. Fang, X. Luo, H. Cai, T. Y. Liow, M. B. Yu, G. Q. Lo, and D. L. Kwong, "Thermo-optical tunable planar ridge microdisk resonator in silicon-on-insulator," Opt. Express 19, pp. 11220 (2011)
[11] Q. Fang, J. Song, T.-Y. Liow, H. Cai, M. B. Yu, G. Q. Lo, D.-L. Kwong; "Ultralow Power Silicon Photonics Thermo-Optic Switch With Suspended Phase Arms," IEEE Photon. Technol. Lett. 23, pp.525-527 (2011)
[12] J. Song, Q. Fang, S. H. Tao, T. Y. Liow, M. B. Yu, G. Q. Lo, and D. L. Kwong , "Fast and low power Michelson interferometer thermo-optical switch on SOI," Opt. Express 16, pp.15304-15311 (2008).